MARLIN: An AI-based ROV System for Detection and Density Mapping of Invasive *Sargassum horneri* in Monterey Bay

Cynthia Zhang
Saratoga, CA, USA
0009-0008-8677-9559

Cassia Dyer Seem
Los Altos, CA, USA
cassyseem@gmail.com

Abstract—Rapidly emerging blooms of Sargassum horneri are jeopardizing kelp forest ecosystems and shoreline biodiversity in Monterey Bay, California. This study introduces MARLIN, an AI-robotics pipeline operating in real-time, for scalable semi-autonomous underwater surveys of marine benthic organisms, such as invasive macroalgae. This study benchmarked the object detection accuracy of a custom-built remotely operated vehicle (ROV) designed to detect S. horneri in its natural habitat. The system was equipped with a 1920 × 1080-pixel resolution low-light video camera, subsea LED lighting, and onboard deep-learning inference. Approximately 700 field images (manually annotated with bounding boxes and class labels) and data augmentation was used to fine-tune a YOLOv8 object detector model. Model performance was evaluated using precision, recall, F1-score, and mean average precision (mAP@0.5). MARLIN reached 92.8% precision, 96.1% recall, and 94.4% F1 score during semi-autonomous field deployment at McAbee Beach under naturally varying underwater visibility conditions. Surveying a 20 m × 40 m transect in 12 minutes, MARLIN produced 816 true positive detection events. The spatial density map highlighted clumped patterns of invasion. MARLIN's ability to navigate transects while running inference onboard and reconstruct quantitative metrics enables rapid and repeatable monitoring of invasive species. The proposed method minimizes dependency on diver surveys, maximizes frequency of monitoring, and provides a customizable framework that can be deployed on other types of macroalgae as well as other invasive species found in Monterey Bay by training additional models.

Keywords— AI-driven, detection, invasive, monitoring, remotely operated vehicle, Sargassum horneri, underwater

I. Introduction

Sargassum horneri is an invasive brown macroalga that has become an ecological menace to temperate kelp forests along the coast of California [1]. This fast-growing alga can outcompete native kelp forests, leading to reduced complexity and altered community structure [1]. Reductions in canopy-forming kelp can be directly measured by a decline in abundance and diversity of invertebrate populations as well as ecosystem stability [1]. *S. horneri* can degrade the quality of marine habitat as it replaces kelp forests by altering food webs and providing lower nutritional quality food sources for consumers [2]. Microscopically, when *S. horneri* made up 75% of the overall diet of abalone, they began to show signs of malnutrition, including damage to the gut tissue and microbiome [2].

Evidence of range expansion has also been studied for this invasive alga, with maximum relative growth rates of adult blade weight reported at approximately 4.46% day^{-1} [3]. Overall, *S. horneri* has expanded its range by roughly 435 miles along the California coast since it was first discovered in 2003 [4]. Fig. 1 displays the invasion hotspots along the U.S. West Coast and an image of a *S. horneri* specimen. The spatial spread of *S. horneri* will continue to contribute to ecosystem degradation and economic losses if not managed [5], especially in susceptible nearshore ecosystems like Monterey Bay which support high levels of biodiversity and commercial fisheries.

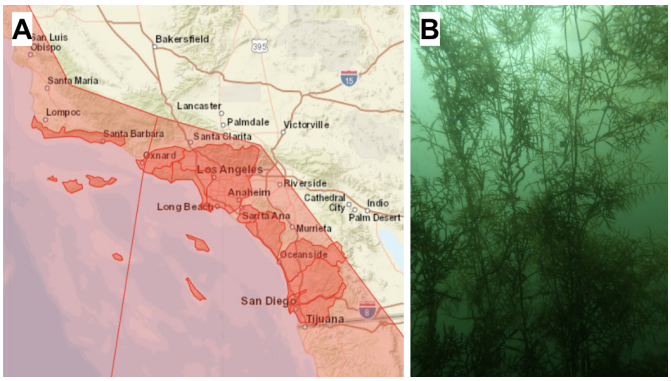


Fig. 1. (A) Geographic distribution of *Sargassum horneri* invasion hotspots along the U.S. West Coast [4]. (B) Underwater photograph of *S. horneri*, an invasive brown macroalga that forms dense stands in nearshore ecosystems.

The impacts of *S. horneri* and control efforts have been recorded by federal and state agencies such as NOAA Fisheries. Several mitigation options have been assessed, such as diver removal, mechanical harvest, and localized removal efforts [6]. These efforts may aid in biomass removal from localized regions but often depend on monitoring efforts to detect *S. horneri* presence and distribution [6]. Currently, most monitoring programs involve diver-based visual surveys. While commonly applied to nearshore ecology assessments, diver-conducted surveillance methods are labor-intensive, costly and spatially limited.

Surveys based on diver observation are restricted by bottom time. Available bottom time for diver-based surveys decreases with depth; NOAA's no-decompression air tables specify maximum no-stop times of 60 minutes at 60 ft [7]. Accounting for descent and ascent time, navigation between waypoints, and time spent conducting scientific surveys leave significantly less time for underwater observations. Using a representative scientific belt-transect swimming speed of approximately 5 m/min, a diver would require about 64 minutes of active swimming to complete the sixteen 20 m passes needed to survey a 20 m × 40

XXX-X-XXXX-XXXX-X/XX/$XX.00 ©20XX IEEE

m area, excluding descent, ascent, transect setup, turns, and other operational time [8]. This leaves little area surveyed per dive and subsequently multiple dive teams and days in the field to survey multiple sites/quadrats. After collecting the data, dive teams must also spend time transcribing their data and reviewing video, along with the tedious work of counting and filtering to determine density. In addition to underwater survey time, diver-based monitoring requires trained personnel, specialized equipment, safety and medical compliance, and potentially vessel support, resulting in substantial operational and logistical demands [9]. These expenses and logistics limit survey repeatability and often preclude the observation of initial colonization events at which point localized control efforts would be most beneficial. Diver-based visual surveys can be influenced by observer experience, species detectability, survey methodology, and environmental conditions such as visibility and current, potentially affecting the accuracy and consistency of abundance estimates [10]. Overall, diver-based visual sampling is limited in scalability, repeatability, and temporal frequency. Currently, there is no widely adopted scalable method capable of recording real-time, spatially explicit presence of *S. horneri*.

Automated detection processes eliminate exhaustive review of imagery by technicians and provide real-time analysis of presence or absence of targeted species. Object detection frameworks based on convolutional neural networks (CNNs), such as You Only Look Once (YOLO) version 8 developed by Ultralytics [11], are fast and effective at classifying objects in high resolution videos (>30 frames per second). Classifying objects directly after collection either in the field or in a laboratory greatly reduces the processing time needed to review survey videos. Automated processing reduces reliance on repeated manual image review and applies a consistent trained model across surveys. With a trained model, entire regions can be surveyed with the same model creating standardized and comparable data between sites longitudinally. Models can be applied repeatedly to new surveys without the need for re-training allowing frequent monitoring at higher temporal resolution which could allow for early detection of invasion events. Coupling marine robotics and autonomous computer vision creates an opportunity for streamlined surveillance of marine ecosystems that could complement diver-based control efforts, as illustrated by the life cycle stages of *S. horneri* shown in Fig. 2.

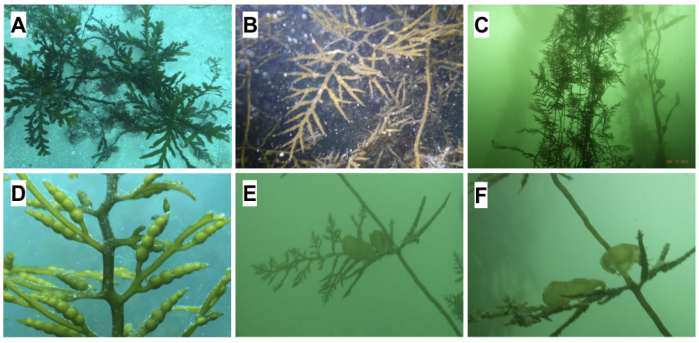


Fig. 2. Life cycle stages of *Sargassum horneri*: (A) sprouting thalli, (B) juvenile stage, (C) mature thallus, (D) early reproductive development, (E) reproductive structures, and (F) drifting thalli following reproduction and detachment.

II. Related Work

A. *Ecological Impacts and Invasion of* Sargassum horneri

Sea temperatures off the coast of California often range 57–72 °F (14–22 °C) [3], overlapping with the thermal range experienced by *S. horneri* populations. The species cultured at higher temperatures reached the recruitment phase faster near 68 °F (~20 °C) [12]. Experimental growth rates at this temperature were reported to increase to ~57%, and surviving individuals also reproduced faster [12]. Recruitment also increased with temperature, so projected ocean warming will potentially increase the competitive advantage of *S. horneri* over canopy-forming kelps. *S. horneri* tolerates temperatures above approximately 18.5 °C and does not lose significant tissue mass during heat wave conditions [13]. Native taxa, such as Macrocystis pyrifera, would typically experience similar stress during these conditions and show reduced growth or decline in canopy. Immature *S. horneri* can reach reproductive age in as little as two weeks [13]. Growth seasonality is also inverted compared to native species, allowing it to occupy space when kelp canopy is less dense. Growth and life cycle progression of *S. horneri* can be seen in Fig. 2.

Increases in water temperature can cause macroalgal assemblages to shift, thereby affecting community ecology. Harrison found that when surveyed, beaches that were dominated by invasive *S. horneri* had different invertebrate compositions than beaches with native canopy kelp species [14]. Both species richness and total invertebrate abundance were higher on patches of native Macrocystis pyrifera than on patches of *S. horneri* [14]. When juvenile abalone were fed a diet of invasive *S. horneri* in replacement of their typical kelp-based diet, they experienced gut tissue damage, changes in microbiota composition, reduced growth, and signs of starvation and malnutrition at a replacement level of over 75% [2]. Therefore, as basal producers shift from native species to introduced and invasive macroalgae, associated ecological impacts may influence wrack-based food webs.

B. *ROV-Based Monitoring and Underwater Object Detection*

There have also been advancements in detecting environmental stressors using marine robotics. Tait et al. compared ROV and diver-based surveillance of nonindigenous marine species [15]. ROVs produced permanent video records and could operate where diving was restricted, whereas divers achieved higher detection rates in the evaluated conditions: approximately 0.5 versus 0.2 nonindigenous species per minute [15]. These results show that ROV surveys offer operational benefits but require improved automated detection to approach diver performance.

While diver-based surveys provide superior image clarity, ROV systems offer a significant advantage in spatial coverage, capable of reconstructing over 11,000 m^2 of seabed in a fraction of the time required for manual diving [16]. Furthermore, ROV-derived photogrammetry has been shown to achieve the millimeter-scale resolution necessary to resolve complex benthic features, making it a more cost-effective and scalable solution for large-scale environmental monitoring and conservation efforts [16].

Beyond simple detection, the optimization of YOLO-based models in marine environments is heavily influenced by image resolution and camera gain [17]. Research on in-trawl imaging has demonstrated that while high-resolution datasets (up to 1216 pixels) significantly improve the detection of small-scale crustaceans, model performance remains variable across different lighting conditions, with white light typically yielding higher precision than red-light alternatives [17].

YOLO-based detectors have also been applied to marine ecological monitoring under challenging underwater imaging conditions. Al Muksit *et al.* developed YOLO-Fish to detect fish in realistic underwater scenes affected by low illumination, complex backgrounds, and substantial variation in object appearance [18]. Xu and Matzner applied YOLO to fish detection in underwater video collected at multiple water-power sites and found that performance decreased when the model was evaluated on imagery from a site excluded from training [19]. These studies demonstrate the suitability of YOLO for low-latency underwater detection while also highlighting the importance of environmental diversity and independent-site validation.

Deep-learning perception has also been integrated directly with ROV imaging systems. Zhang *et al.* proposed a class-weighted YOLO method for detecting and tracking objects in underwater photographs captured by ROVs, addressing challenges including image blur, scale variation, complex backgrounds, and unequal sample difficulty [20]. Their work demonstrated the feasibility of applying real-time object detection to ROV imagery, but it focused primarily on improving detection and tracking rather than coupling species-specific detection with field-scale density mapping.

Prior studies have demonstrated underwater YOLO detection and AI-enabled perception on ROV platforms, but few have combined onboard, species-specific inference with spatial density mapping during field surveys. No published system identified in this review was designed specifically for real-time detection and mapping of *S. horneri*. MARLIN was therefore developed as a semi-autonomous ROV system that integrates YOLO-based detection, transect navigation, and spatial mapping for field monitoring of this invasive macroalga.

During deployment, MARLIN processed video onboard and used validated detections to generate spatial density maps of the surveyed area. This approach reduces post-survey image review and provides a repeatable framework that may be adapted to additional marine species through model retraining.

III. Methodology

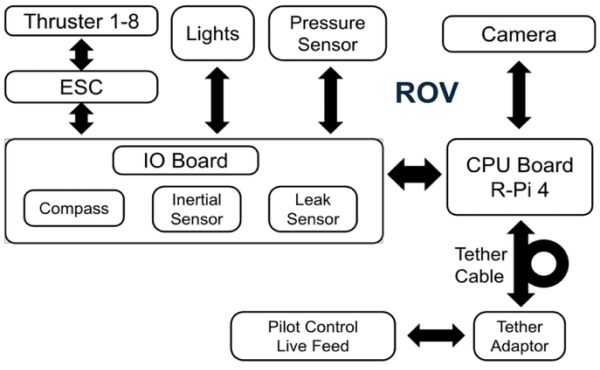


Fig. 3. Electrical system diagram of the MARLIN ROV showing onboard sensors, thrusters, camera, and control architecture.

A. MARLIN System Design

MARLIN was designed with hardware specifications capable of providing quantitative imagery while supporting semiautonomous operation for independent seabed surveying of invasive macroalgae in nearshore environments. A detailed block diagram of MARLIN hardware components is shown in Fig. 3. The components include sensing and navigation, thrust and propulsion, computing, and control systems. MARLIN utilizes eight omnidirectional thrusters (~5.1 kgf thrust each) for directional control, electronic speed controllers (ESCs) for thruster management, a Raspberry Pi (RPi) 4 CPU board, and tethered vehicle-to-pilot communication system. Configuration of these systems allows for teleoperation of MARLIN as well as closed-loop feedback during semiautonomous travel to persistently image under conditions with varying current strengths and turbidity. Hardware acceleration of object detection required enabling reliable visual recognition. MARLIN is equipped with a low-light, HD USB camera which can stream video at 1920 × 1080-pixels resolution. Continuous video streaming enables frame capture for real-time object detection. Coastal waters have significant light attenuation and experience frequent occurrences of suspended sediment. To increase illumination within the marine environment and strengthen the signal-to-noise ratio (SNR) of captured video, subsea LED lights were installed. Pose information from a gyrocompass and inertial measurement unit (IMU) mounted on board the vehicle was used to compensate imagery used with bounding-box-based object detection models.

Vehicle depth was monitored using a pressure-based depth sensor. Longitude and latitude were estimated during traveled paths to provide rough estimates of traveled distance during transects and allow for reproducible geometry between deployments. A fixed camera-to-target distance allows for less variability in scale within imagery and promotes model consistency during inference. Computational hardware was selected with onboard inference in mind to decrease required bandwidth across the tethered cable and facilitate real-time object detection while in the field. The resulting computer vision architecture allowed for near-zero latency inference while also allowing access to raw imagery for postprocessing verification. Several constraints were placed on the vehicle design to promote safe operation, reproducibility of the methodology, and production cost below $1,500. The operational maximum diving depth was set to 100 ft to encapsulate the vertical range of *S. horneri* found in Monterey Bay. The horizontal range of the tether permitted operations up to ~500 ft from the pilot system. Low-cost commercial parts were used to maximize accessibility of this technology to other laboratories. Using commercial off-the-shelf parts allowed for ease of replacement should a component fail and promotes reproducibility of this study. Designed battery life allows for 3-4 hours of continuous operation on a single battery charge under typical use. MARLIN was deployed with these constraints in mind and can be seen in Fig. 4.

Waterproof enclosures, cable penetrators, and thrusters were obtained commercially from Blue Robotics, while the remaining frame, computing, and electrical components were assembled from commercially available parts.

TABLE I. SOFTWARE DEVELOPMENT TOOLS

Tool	Purpose
Python	Data preparation, model execution, and analysis
Ultralytics Yolov8	Object-detector training, validation, and inference
PyTorch	Deep-learning backend
OpenCV	Frame extraction and image processing
Roboflow	Image annotation and dataset management
NumPy	Numerical processing
Pandas	Detection organization and analysis
Matplotlib	Spatial map visualization
ArduPilot	Vehicle control, sensor calibration, and stabilization

B. MARLIN Testing and Validation

MARLIN's waterproof integrity was tested with a vacuum leak test prior to every dive. The sealed electronics case was attached to a manual vacuum pump and depressurized to approximately 15 inHg below atmospheric pressure. By depressurizing the enclosure, pressure differentials like those experienced during submersion are simulated. This also allows verification that there are no leaks before deploying. Internal enclosure pressure was logged for approximately 10 minutes. If the pressure increased by less than 0.5 Hg during the testing period, the O-rings, cable seals, and enclosure were assumed to be correctly sealed. If the case did not pass, it was resealed and tested again. This helps eliminate the possibility of water damage, short circuiting, and loss of onboard instrumentation.

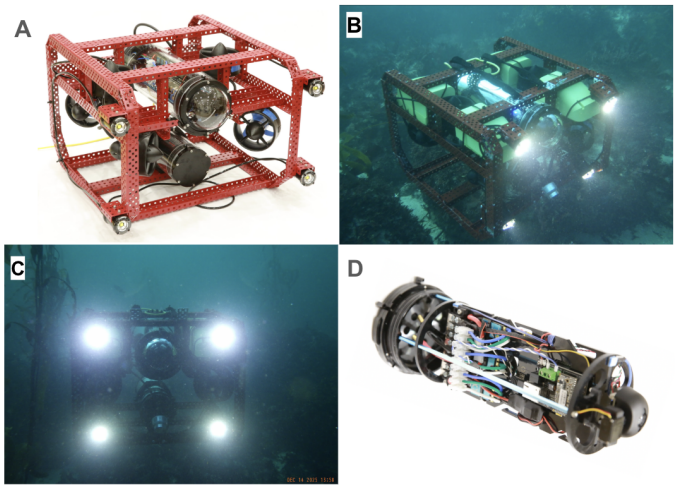


Fig. 4. MARLIN ROV platform and electronics. (A) Oblique front view of the ROV. (B) Underwater right-side view with lighting. (C) Frontal underwater view during deployment. (D) Internal electronics and circuitry.

Sensor calibration was performed prior to each field experiment to ensure consistent navigation and data collection. Sensor calibration was completed through ArduPilot software. Calibration of the compass was completed by spinning MARLIN in several positions along all three axes (yaw, pitch, roll). This helped to remove distortions in the compass reading created by the internal wiring and structure of MARLIN. Calibration of the IMU helped remove bias from gyroscope drift. MARLIN was placed in several positions while stationary to calibrate the accelerometers ensuring that they were aligned with gravity. Zero depth was recorded at the surface pre-deployment to create a consistent pressure reference. Finally, MARLIN was spun in several positions along all three axes to verify that the sensors were producing consistent and steady readings while in motion. Calibration ensures straight transects with less heading drift and steady camera orientation. Correct depth and attitude information allows maintenance of a consistent camera-to-target distance while imaging, allowing for stable detection and spatial mapping of *S. horneri*.

C. ML Model Development

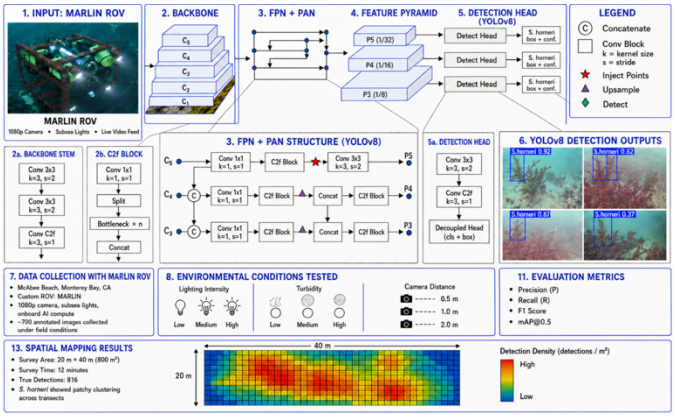


Fig. 5. MARLIN YOLOv8s detection and spatial-mapping workflow, including input imagery, the backbone, FPN/PAN feature aggregation, detection heads, representative inference outputs, field conditions, evaluation metrics, and density-map generation. YOLOv8 architecture diagram was adapted from [21] and modified by the authors.

The YOLOv8 architecture was used for object detection (Fig. 5). Training was initialized from YOLOv8s weights pretrained on the COCO dataset and fine-tuned on the annotated *S. horneri* dataset. YOLOv8 was chosen because it achieves a high frame rate while still maintaining accuracy on the species of interest, enabling it to be deployed on-board edge computation devices. Detection algorithms require low latency to process frames on-board robots for near real-time spatial distribution mapping, as seen in Fig. 6. YOLOv8 utilizes a single shot detector architecture with a feature pyramid network (FPN) and multiple prediction heads for detecting objects at different scales, which is useful for handling close-ups and far away objects during data collection. The training dataset included approximately 700 images with bounding box coordinates and class labels for *S. horneri* (Fig. 7). The dataset was divided into training, validation, and test subsets using a 70%/15%/15% split. Images were captured during different lighting conditions, water clarity, and camera angles. Training images were collected across multiple field deployments in different Monterey Bay locations, encompassing variation in substrate, illumination, turbidity, viewing distance, and surrounding macroalgal communities. However, the quantitative field evaluation reported in this study was conducted on a single 20 m × 40 m transect at McAbee Beach.

YOLOv8 model uses images resized to (640 × 640). Although the input images were provided at a resolution of 1920 × 1080, YOLO internally rescaled them to an effective resolution of approximately 640 × 360, resulting in a loss of spatial detail.

To mitigate this limitation, the dataset preparation pipeline was redesigned to incorporate image tiling. Each original image was divided into two square tiles: a left tile and a right tile, each with dimensions of 1080 × 1080 pixels. The tiles overlapped horizontally by 240 pixels to preserve object continuity across tile boundaries. The overlapping tiles were used only during dataset preparation and model training to preserve image detail and object continuity near tile boundaries. By retaining more source-image detail before resizing to the model input, tiling increased the pixel area occupied by small or distant colonies and made their visual features more available to the detector during training. During field deployment, the same tiling strategy was applied to the live video stream. Predictions from each tile were transformed back into full-frame coordinates, and duplicate detections within the overlapping region were removed using non-maximum suppression (NMS).

A batch size of 2 was used for training. The model was trained for up to 120 epochs with early stopping based on validation performance. The checkpoint with the best validation performance was retained for evaluation. During each epoch, model parameters were updated iteratively over minibatches using the bounding-box regression loss, classification loss, and distribution focal loss implemented by Ultralytics YOLOv8. The model was optimized using AdamW, with an initial learning rate of 0.001, momentum of 0.937, and weight decay of 0.0005. Training augmentation included HSV-based color variation ($h = 0.015$, $s = 0.4$, $v = 0.2$), rotations up to 20°, horizontal flipping with probability 0.5, translation of 0.05, and scaling of 0.5. A confidence threshold of 0.25 was used during field deployment to reduce low-confidence detections while maintaining high recall. This threshold also maintained high recall, which was prioritized because visually similar macroalgae occur near *S. horneri* and missed detections of small colonies are more consequential than additional false positives.

As shown in Fig. 8, the training losses decreased steadily, whereas the validation losses reached their lowest values earlier and subsequently increased. Therefore, the checkpoint with the best validation performance was retained rather than the final-epoch checkpoint.

For field evaluation, a true positive (TP) was a model detection correctly corresponding to visible *S. horneri*, a false positive (FP) was a detection assigned to a non-target organism or background feature, and a false negative (FN) was visible *S. horneri* missed by the model. Ground truth for the field-deployment footage was established through joint frame review by the authors and a Monterey Bay subject-matter expert familiar with local macroalgal identification, who assisted in confirming *S. horneri* and distinguishing it from visually similar species. The reviewed frames were then used to calculate precision, recall, and F1 score. Training images, however, were selected and annotated by the authors without independent expert review.

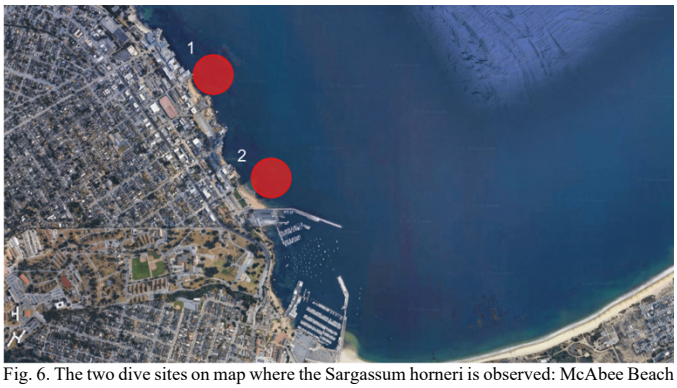


Fig. 6. The two dive sites on map where the Sargassum horneri is observed: McAbee Beach (1) and Breakwater Beach (2). ROV deployment and data collection was done at McAbee Beach.

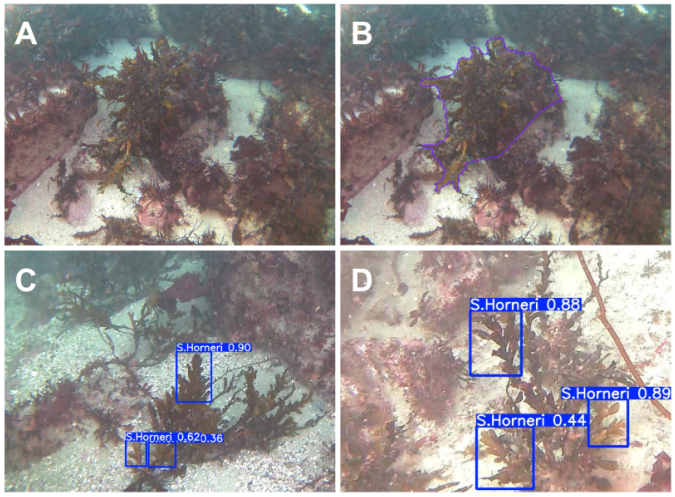


Fig. 7. The training and detection workflow for *Sargassum horneri* using a YOLOv8 model. (A) An unprocessed image taken by MARLIN, (B) labeled training image with a ground-truth annotation, (C, D) YOLOv8 inference outputs displaying bounding-box detections.

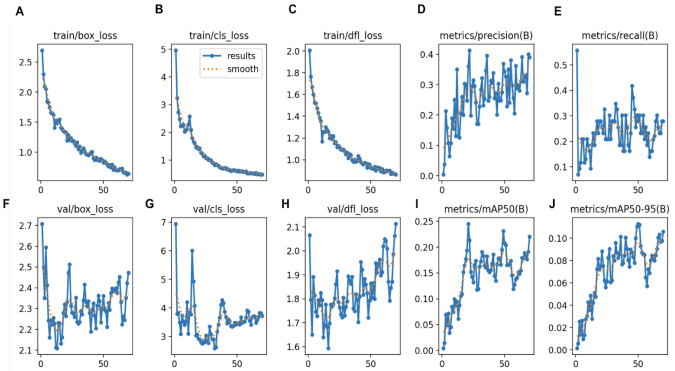


Fig. 8. Training and validation curves for bounding-box loss, classification loss, and distribution focal loss, together with validation losses, precision, recall, mAP@0.5, and mAP@0.5:0.95. This was taken during model development and is separate from the field-deployment evaluation reported in Section IV.

IV. Results and Discussion

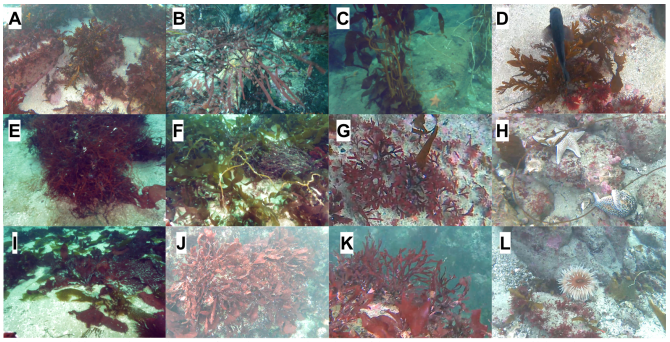


Fig. 9. Different invasive and native species found in Monterey Bay, California: Sargassum horneri (A), Dasysiphonia japonica (B), Undaria pinnatifida (C), Rosylip sculpin (D), Dasysiphonia japonica (E), Gracilaria vermiculophylla (F), Grateloupia turuturu (G), Tubastraea coccinea (H), Grateloupia turuturu (I-J), Dasysiphonia japonica (K), and Anthopleura hermaphroditica (L).

MARLIN completed its navigation along a 20 m × 40 m transect within 12 minutes at a known location of *Sargassum horneri* at McAbee Beach in Monterey Bay. MARLIN followed a lawnmower-like path, achieving complete area coverage by traversing sixteen 20 m long paths parallel to one another. MARLIN maintained a roughly constant altitude and forward speed along each pass, achieving an approximately uniform sampling density. Underwater video was captured during navigation (see examples in Fig. 9). Inference occurred onboard during the navigation task in ambient environmental conditions with field-realistic turbidity and illumination.

The vehicle detected 816 true positives of *S. horneri* along the transect. Dividing by the total area swept, MARLIN observed an approximate density of 1.02 objects for m². Locations of detections were estimated from the transect position estimates and rasterized into a density map (Fig. 10). This map reveals localized regions of high density along parts of the transect and low density along neighboring regions. These variations in object density could be a signal of patchy invasion: smaller areas where organisms have settled and begun to grow, depending on the characteristics of the substrate or other available microhabitat. As shown from the strip heatmap overlaid on the transect track in Fig. 10C, there also exists variation in detections both vertically along the transect strip and horizontally between transects within each 20 m × 40 m area plot. This local variability highlights the spatial intricacies of invasion that may not be captured by divers sampling quadrats. MARLIN's coverage of 800 m² in 12 minutes exceeds the survey rate typically reported for manual diver-based surveys (~64 min for 800 m² plot). Structuring navigation around concurrent onboard inference enabled MARLIN to infer targets in near-real time without post-processing of captured video. Furthermore, this rate of coverage allowed the ROV to complete stable imaging along each pass with minimal sediment resuspension.

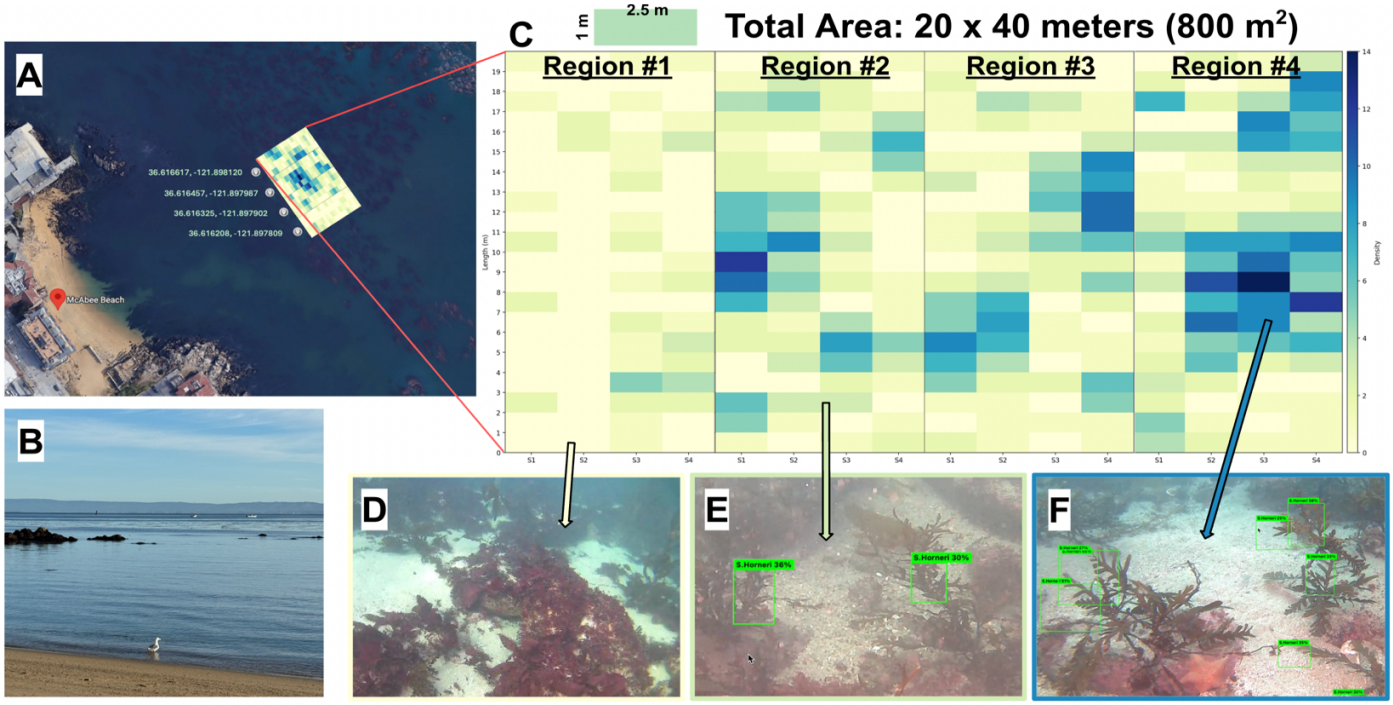


Fig. 10. Spatial density mapping of *S. horneri*. (A–B) Survey site at McAbee Beach, Monterey Bay. (C) Detection heatmap across transects. (D-F) Example regions with 0, 2, and 5 detections, respectively.

During field evaluation, the model obtained 816 TP, 63 FP, and 33 FN from the total area surveyed (800 m²). These statistics translate to a precision of 92.8%, recall of 96.1%, and an F1 score of 94.4%.

TABLE II. False Positive Error Breakdown

FP Source	Count	Percentage of all FP
Other Brown Macroalgae	15	23.8%
Benthic Organisms	5	7.9%
Substrate/Debris	32	50.8%
Imaging Artifacts	11	17.5%

TABLE III. False Negative Error Breakdown

FN Source	Count	Percentage of all FN
Motion Blur	5	15.2%
Debris	13	39.4%
Low Illumination or Contrast	3	9.1%
Small or Distant Target	10	30.3%
Partial Obstruction	2	6.1%

The high recall rate suggests that most visible individuals of *S. horneri* within the FOV were detected successfully. For invasive species detection, having a high recall is critical as false negatives represent missed detection. The precision of the model held relatively well under natural conditions in the water column. False positives were generally caused by macroalgae or benthic life that had similar coloring, branching shapes, and textures as *S. horneri*. False negatives were generally due to motion blur when the vehicle was turning, algae being partly covered by sediment or other macroalgae, or poor lighting conditions creating low contrast between *S. horneri* and the background. Most false negatives occurred around where the segments switched to create the lawnmower pattern, as small changes in angle of the vehicle caused differences in shadows which created less defined edges. Overall, the model had consistent performance between transects indicating that the pipeline was able to generalize well in varying turbidity and lighting conditions. The F1 score was 94.4%, suggesting that there was a good balance between precision and recall and that the model was able to detect organisms reliably during active vehicle motion. These metrics were calculated during an actual deployment, not from testing in a laboratory setting. This suggests that YOLOv8 is able to detect the presence of *S. horneri* with high sensitivity in the field.

Performance may degrade at new sites because of domain shifts in turbidity, illumination, water color, wave-induced camera motion, substrate type, imaging distance, and the abundance of visually similar macroalgae. These changes can alter object contrast, apparent scale, color, and background texture relative to the training data. Additional evaluations are ongoing at other Monterey Bay sites to quantify site-to-site performance and determine whether broader training data or site-specific adaptation is required.

Coverage maps exhibited clumping behavior, which can be attributed to *S. horneri* not being uniformly distributed across the sampling region. However, these aggregations of detections, or patches, can be used to delineate areas of colonization. Identifying such clusters may help characterize spatial patterns of colonization and support targeted monitoring or removal. Populations of invasive species often cluster early on because their reproductive propagules settle in ideal areas with suitable substrate, sunlight, or low competition. Mapping these densities provides analysts with the ability to understand heterogeneity in the sampled population - there can be patches of high and low infestation even within a relatively small survey area (20 m × 40 m). If management of the species is needed, mapping allows for targeted management of localized infestation patches.

High recall was prioritized intentionally to ensure as many true positives as possible were captured in order to prevent false negatives. Precision was moderate (92.8%) because backgrounds and morphological features between macroalgae species can appear very similar. However, false positive detections pose a much lower risk than false negatives in invasive species monitoring. The confidence threshold was selected to favor recall, accepting additional false positives in exchange for fewer missed detections. The deployed system obtained a strong F1 score of 94.4%. Travel paths paired with onboard inference allow for consistent mapping of transects of species distributions. Instead of having divers swim an area and log what they find, there is less bias and consistent time intervals can be used between repeat deployments to monitor growth. Sampling with an ROV also allows surveys to be done in clearer water than is possible with scuba because diver fins can disturb sediment in shallow regions. Field deployment was also able to operate for roughly three to four hours due to the battery system, providing substantially more coverage than the typical one-hour dive window.

Hardware improvements including better lighting and more thrusters allowed for more precise ROV piloting. Additional rotational thrusters allowed the ROV to make sharper turns without forward drift while repositioning itself. Better lighting allowed for greater image contrast and edge definition, allowing for better detection confidence. ROV deployment lessens the likelihood of diver-induced disturbance to fragile ecosystems and can be used to monitor environments that may be dangerous to humans. For these reasons, AI-enabled ROV technology should be used to aid scientists in data collection, complementing traditional diver-based surveys.

V. Conclusion

MARLIN has been successfully developed and deployed for detection of the invasive macroalga *Sargassum horneri*. Upon traversing a 20 m × 40 m field test area, MARLIN correctly detected 816 instances of the target species. MARLIN exhibits promising in-field performance with 92.8% precision, 96.1% recall, and an F1-score of 94.4% while accounting for environmental noise. The system performance demonstrated semi-autonomous detection in field settings and can be used for real-time detection applications and can be trained to detect other marine organisms. Spatial point reconstructions from MARLIN allow quantitative density estimates and detection of fine-scale spatial heterogeneity across invasion fronts. In addition to broadscale occupancy estimates, point-reconstructed datasets offer localization of spatial clusters. Potential applications of ecological relevance include improving removal efforts and informing decisions based on data. Locomotion over user-defined transects couples inferencing capabilities on-board MARLIN to decrease diver dependence and perform repeatable surveys with decreased disturbance to the benthic environment. Field-deployable ML-assisted average target recall (ATR) demonstrates promising capabilities to quickly survey discretized spaces with high recall, beneficial for early detection when loss of an invasive species-free area may be consequential to ecosystem health. With larger training datasets, robust localization, and fully autonomous navigation, there is potential for ML-equipped robots to assist with repeatable, quantitative monitoring of ecosystems and enable early-warning detection

of invasive species across diverse marine habitats. Future versions of MARLIN could also be trained to locate juvenile *S. horneri*, and a removal mechanism could then be integrated into the ROV so that detected individuals could be targeted and removed during the same survey.

References

[1] L. M. Marks, "The distribution, biology and ecology of the invasive seaweed *Sargassum horneri* in its introduced range," Ph.D. dissertation, Univ. California, Santa Barbara, Santa Barbara, CA, USA, 2018. [Online]. Available: ProQuest Dissertations & Theses Global, ProQuest document ID 2038559523.

[2] S. Hur *et al.*, "Dietary replacement of Undaria pinnatifida by Sargassum horneri in feed formulation for abalone Haliotis discus hannai: Effect on growth, gut microbiota, and taste sensory profile," *Frontiers in Marine Science*, vol. 10, Feb. 2023, doi: https://doi.org/10.3389/fmars.2023.1053240.

[3] L. Marks *et al.*, "Range expansion of a non-native, invasive macroalga Sargassum horneri (Turner) C. Agardh, 1820 in the eastern Pacific," *BioInvasions Records*, vol. 4, no. 4, pp. 243–248, Nov. 2015, doi: https://doi.org/10.3391/bir.2015.4.4.02.

[4] Smithsonian Environmental Research Center, "*Sargassum horneri*," *National Exotic Marine and Estuarine Species Information System*, 2024. [Online]. Available: https://invasions.si.edu/nemesis/species_summary/-449.

[5] D. Jin, A. Wang, and T. Dalton, "Economic impacts of sargassum events in Puerto Rico, USVI, and coastal Florida," *Harmful Algae*, vol. 150, Art. no. 102996, Dec. 2025, doi: 10.1016/j.hal.2025.102996.

[6] L. M. Marks, D. C. Reed, and A. K. Obaza, "Assessment of control methods for the invasive seaweed *Sargassum horneri* in California, USA," *Management of Biological Invasions*, vol. 8, no. 2, pp. 205–213, 2017, doi: 10.3391/mbi.2017.8.2.08.

[7] National Oceanic and Atmospheric Administration, "NOAA no-decompression table: Multiple air dives." [Online]. Available: NOAA Office of Marine and Aviation Operations. Accessed: Jul. 23, 2026.

[8] Department of Conservation, *Underwater Transects for Sampling Reef Fishes, Version 1.0*, Inventory and Monitoring Toolbox: Marine, New Zealand Government, 2017. [Online]. Available: Department of Conservation. Accessed: Jul. 23, 2026.

[9] R. McGeady *et al*., "A review of new and existing non-extractive techniques for monitoring marine protected areas," *Frontiers in Marine Science*, vol. 10, 2023, doi: 10.3389/fmars.2023.1126301.

[10] G. J. Edgar, N. S. Barrett, and A. J. Morton, "Biases associated with the use of underwater visual census techniques to quantify the density and size-structure of fish populations," *Journal of Experimental Marine Biology and Ecology*, vol. 308, no. 2, pp. 269–290, Sep. 2004, doi: 10.1016/j.jembe.2004.03.004.

[11] G. Jocher, A. Chaurasia, and J. Qiu, "Ultralytics YOLOv8," version 8.0.0, 2023. [Online]. Available: https://github.com/ultralytics/ultralytics

[12] S. L. Small and M. S. Edwards, "Thermal Tolerance May Slow, But Not Prevent, the Spread of *Sargassum horneri* (Phaeophyceae) along the California, USA and Baja California, MEX Coastline," *Journal of Phycology*, vol. 57, no. 3, pp. 903–915, Apr. 2021, doi: https://doi.org/10.1111/jpy.13148.

[13] M. J. Andersen, "El Niño conditions facilitate invasion of the non-native seaweed Sargassum horneri into San Diego's kelp forests," *Escholarship.org*, 2022. https://escholarship.org/uc/item/3sw1m7g9

[14] L. N. Harrison, "Changes in sandy beach invertebrate communities driven by an invasive macroalga, *Sargassum horneri*," Master's thesis, Dept. Biol., San Diego State Univ., San Diego, CA, USA, 2022.

[15] L. W. Tait *et al.*, "Towards remote surveillance of marine pests: A comparison between remote operated vehicles and diver surveys," *Frontiers in Marine Science*, vol. 10, Mar. 2023, doi: https://doi.org/10.3389/fmars.2023.1102506.

[16] I. L. R. Paterson, K. E. Dawson, A. O. M. Mogg, M. D. J. Sayer, and H. L. Burdett, "Quantitative comparison of ROV and diver-based photogrammetry to reconstruct maerl bed ecosystems," *Aquatic Conservation: Marine and Freshwater Ecosystems*, vol. 34, no. 11, Art. no. e70007, Nov. 2024, doi: 10.1002/aqc.70007.

[17] T. Westergerling, V. Allken, W. Melle, A. G. V. Salvanes, and S. Rosen, "A deep learning-based model for automatic identification of mesopelagic organisms from in-trawl cameras," *PLOS One*, vol. 21, no. 1, p. e0340640, Jan. 2026, doi: https://doi.org/10.1371/journal.pone.0340640.

[18] A. A. Muksit, F. Hasan, M. F. H. B. Emon, M. R. Haque, A. R. Anwary, and S. Shatabda, "YOLO-Fish: A robust fish detection model to detect fish in realistic underwater environment," *Ecological Informatics*, vol. 72, Art. no. 101847, Dec. 2022, doi: 10.1016/j.ecoinf.2022.101847.

[19] W. Xu and S. Matzner, "Underwater fish detection using deep learning for water power applications," in *Proc. Int. Conf. Comput. Sci. Comput. Intell. (CSCI)*, Las Vegas, NV, USA, 2018, pp. 313–318, doi: 10.1109/CSCI46756.2018.00067.

[20] L. Zhang, C. Li, and H. Sun, "Object detection/tracking toward underwater photographs by remotely operated vehicles (ROVs)," *Future Generation Computer Systems*, vol. 126, pp. 163–168, Jan. 2022, doi: 10.1016/j.future.2021.07.011.

[21] J. Terven, D. M. Córdova-Esparza, and J.-A. Romero-González, "A comprehensive review of YOLO architectures in computer vision: From YOLOv1 to YOLOv8 and YOLO-NAS," *Machine Learning and Knowledge Extraction*, vol. 5, no. 4, pp. 1680–1716, 2023, doi: 10.3390/make5040083.